Microchimica Acta (2023) 190:262
https://doi.org/10.1007/s00604-023-05842-8

ORIGINAL PAPER

A novel molecular imprinted QCM sensor based on MoS_2NPs-MWCNT nanocomposite for zearalenone determination

Nesrin Çapar[1] · İlknur Polat[1] · Bahar Bankoğlu Yola[2] · Necip Atar[3] · Mehmet Lütfi Yola[1]

Received: 9 March 2023 / Accepted: 24 May 2023 / Published online: 17 June 2023

Abstract

Zearalenone (ZEN) is a mycotoxin that has a carcinogenic effect and is often found at a high rate in frequently consumed foods. In this study, a characteristic molecular imprinted quartz crystal microbalance (QCM) sensor based on molybdenum disulfide nanoparticle (MoS_2NPs)-multiwalled carbon nanotube (MWCNT) nanocomposite (MoS_2NPs-MWCNTs) is presented for selective determination of ZEA in rice samples. Firstly, molybdenum disulfide nanoparticle (MoS_2NP)-multiwalled carbon nanotube nanocomposites were characterized by using microscopic, spectroscopic, and electrochemical techniques. Then, ZEA-imprinted QCM chip was prepared in the presence of methacryloylamidoglutamicacid (MAGA) as monomer, N,N′-azobisisobutyronitrile (AIBN) as initiator, and ZEA as target molecule by using UV polymerization. The sensor revealed a linearity toward ZEA in the range 1.0–10.0 ng L^{-1} with a detection limit (LOD) of 0.30 ng L^{-1}. The high repeatability, reusability, selectivity, and stability of the developed sensor enable reliable ZEA detection in rice samples.

Keywords Zearalenone · Molecularly imprinting · Nanocomposite · Quartz crystal microbalance · Food analysis

Introduction

Mycotoxins are secondary metabolites produced by filamentous fungi (molds) in food and feed products, mainly from cereals. These low-molecular-weight compounds can exert a range of toxic effects against microorganisms, animals, and humans. In addition, mycotoxins are common contaminants of food sources such as wheat, barley, maize, and rice and pose a risk to human and animal health [1, 2]. ZEA is a mycotoxin produced by various *Fusarium* species. ZEA is a common mycotoxin in corn, wheat, barley, rye, and other grains. Cereal-based products such as cereals, ground cereal products, breakfast cereals, baby foods, corn germ oil, and wheat germ oil are also accepted as the main sources of ZEA exposure for humans. ZEA exposure has been associated with various diseases such as various cancers, cardiovascular diseases, neurological disorders, and asthma [3, 4]. In literature, the chromatographic methods such as high liquid pressure chromatography (HPLC), liquid chromatography–mass spectrometry (LC–MS), and gas chromatography–mass spectrometry (GC–MS) were developed for mycotoxins detection in real samples [5–7]. However, it can be said that analyses are not carried out with an environmentalist approach, since these methods involve excessive specialization, pre-processing, and excessive chemical consumption. Hence, there is a need for especially sensor based on piezoelectric effect such as QCM that can provide ZEA detection more sensitively for reliable food consumption. The piezoelectric effect as a physical theory can enable voltage on mechanical stress. A piezoelectric crystal as a sensor platform can perform on the principle of oscillation change [8]. QCM is a piezoelectric crystal and operates at frequencies below 15 MHz. Quartz is common crystal type in analytical applications due to its diverse features [9].

Carbon nanotubes have recently started to be used as a surface material in sensor technology such as nanotechnology due to their physical, chemical, electronic, and surface area properties [10, 11]. Especially since carbon nanotubes accelerate both surface conductivity and electron transfer, its importance is increasing in sensor applications [12]. In

✉ Mehmet Lütfi Yola
mlutfi.yola@hku.edu.tr

[1] Department of Nutrition and Dietetics, Faculty of Health Sciences, Hasan Kalyoncu University, Gaziantep, Turkey

[2] Department of Engineering Basic Sciences, Faculty of Engineering and Natural Sciences, Gaziantep Islam Science and Technology University, Gaziantep, Turkey

[3] Department of Chemical Engineering, Faculty of Engineering, Pamukkale University, Denizli, Turkey

addition, carbon nanotubes have superior mechanical properties because sp^2 hybridization in carbon nanotubes creates a stronger bonding form than sp^3 hybridization in diamond [13]. Metal dichalcogenides with a layered structure such as SnS_2 and MoS_2 have been used frequently in sensor technology in recent years due to their optical and electronic properties [14, 15].

Each crystal layer of MoS_2 consists of a separate layer of molybdenum atoms, and each layer of molybdenum consists of two layers of sulfur atoms. Atoms lying in the same crystal layer are closely packed and strongly bonded to each other, but each layer is far apart and slides easily over one another due to weak Van Der Waals bonds [16, 17]. MoS_2 is frequently used in different applications such as catalysis, supercapacitor, and battery due to its electronic properties [18]. However, the limited electronic properties of MoS_2 compared to graphene and carbon nanotubes make it rarely used alone in sensor applications [18]. Thus, the controlled doping or complex formation improves the electronic properties of MoS_2 and causes it to be used as electrode material. For instance, polypyrrole/MoS_2 [18] and graphene/MoS_2 [14] composites were utilized as electrode materials in supercapacitor and voltammetric sensor applications.

The process of creating cross-linked and specific polymeric structures for the target molecule is called as molecular imprinting. For the molecular imprinting process, a prepolymerization complex is formed by the interaction of the functional monomer and the analyte. After that, polymerization is initiated by the addition of the crosslinker. Thanks to the excess of the crosslinker, the functional groups of the functional monomer and the analyte are frozen. As a result of the removal of the analyte from the structure, a recognition region of a completely analyte-specific shape and size is obtained. The molecular imprinted polymer (MIP) has analyte-specific molecular recognition sites and is ready to interact with high affinity. In recent years, we have seen that MIPs are used as recognition elements in sensor technology [19–21].

This paper provides the efficient detection method based on MIP and QCM chip for ZEA recognition based on MoS_2NPs-MWCNTs. QCM are piezoelectric devices including a thin quartz plate with gold electrodes attached to both sides of the piezoelectric transducers. Quartz is the most widely used piezoelectric material because of its resistance to thermal, chemical, and mechanical stress. A key advantage of QCM sensors is that they can be used as sensor devices without the need for labeling agents. In addition, QCM sensors have important advantages such as being cheap and small, allowing to work with very small samples, cost-effectiveness, enabling on-site measurements, simplicity of methods, repeatability, ease of design, and high sensitivity. The prepared MoS_2NP-MWCNT nanocomposite indicated a specific surface area toward analyte molecule and superior sensor performance. The produced MIP-based QCM sensor will not only provide a new perspective for detecting mycotoxins but will also be a tool for more reliable food consumption and healthy living.

Experimental

Materials

ZEA, aflatoxin B1 (AFB1), fumonisin B1 (FB1), ochratoxin A (OTA), 2-hydroxyethylmethacrylate (HEMA), MAGA, ethylene glycol dimethacrylate (EGDMA), AIBN, sodium chloride (NaCl), MWCNTs (with 35–45 nm in diameter), sodium molybdate dihydrate ($Na_2MoO_4.2H_2O$), cetyltrimethylammonium bromide (CTAB), and L-cysteine were maintained by Sigma-Aldrich. Phosphate-buffered saline (pH 6.0, PBS) (0.1 mol L^{-1}) was chosen as a supporting solution.

Instrumentation

SEM, TEM, XRD, FTIR, and AFM methods were employed for the characterizations of MoS_2NPs-MWCNTs and MoS_2NPs (see Supplementary Data). Gamry Reference 600 workstation was performed for the electrochemical investigations by using electrochemical impedance spectroscopy (EIS) and cyclic voltammetry (CV). QCM system (INFICON Acquires Maxtek) was performed for ZEA recognition.

Preparation of MoS_2NPs-MWCNTs and MoS_2NPs

Preparation of MoS_2NPs-MWCNTs and MoS_2NPs was carried out by a hydrothermal approach [22]. After the preparation of the mixture including in MWCNTs (0.10 g) and CTAB (100.0 mg) as cationic surfactant providing homogeneous dispersion in ultra-pure water (50.0 mL) at 25 °C, $Na_2MoO_4.2H_2O$ (0.30 g) was slowly added into above dispersion for 45 min. Then, pH of the dispersion was adjusted to 7.0, and L-cysteine (0.50 g) was added into the resultant dispersion. After the transportation of the resultant dispersion into Teflon steel autoclave, the temperature was maintained at 150 °C for 10 h, providing *MoS_2NP-MWCNT* nanocomposite. Same procedure was applied to the preparation of *MoS_2NPs* without introducing MWCNTs.

QCM chip modification with MoS_2NP-MWCNT nanocomposite and the production of ZEA-imprinted QCM sensor based on MoS_2NPs-MWCNTs

The gold surfaces of QCM chips were firstly cleaned by leaving them in acidic piranha solution (50.0 mL, 3:1 H_2SO_4:H_2O_2, v/v) in the agitated bath system for 45 min.

After the drying process under nitrogen atmosphere for 45 min, the prepared nanocomposite solution (5.0 mg mL^{-1}) was dripped onto the gold surface and the modification process was started by means of gold–sulfur affinity for 30 min, providing *MoS_2NPs-MWCNTs/QCM* [9].

After complex formation was completed in the presence of PBS (1.0 mL, pH 6.0) for 1 h between MAGA and ZEA in the ratio (2:1), a dispersion containing AIBN (5.0 mg) and EGDMA (2.0 mL) was prepared. Then, ZEA-MAGA complex (1.0 mL) was slowly added into AIBN-EGDMA solution (1.0 mL) for 2 h. After passing nitrogen gas into this final dispersion for about 30 min, this resultant solution (40.0 µL) was dripped onto MoS_2NPs-MWCNTs/QCM by spin-coating method for 10 s and dried at 25 °C for 45 min. After UV polymerization by UV light (365 nm) for 25 min, ZEA-imprinted QCM chip based on MoS_2NPs-MWCNTs was prepared (*MIP/MoS_2NPs-MWCNTs/QCM*). In the same way, ZEA-non-imprinted QCM chip based on MoS_2NPs-MWCNTs was prepared without analyte molecule to reveal the imprinting selectivity (*NIP/MoS_2NPs-MWCNTs/QCM*).

ZEA removal from MIP/MoS_2NPs-MWCNTs/QCM

In order to break the electrostatic interactions between MAGA and the analyte molecule, after the prepared MIP/MoS_2NPs-MWCNTs/QCM chip was placed in a flask containing 2.0 mol L^{-1} NaCl (30.0 mL), ZEA molecule was removed from the chip with the help of a shaking bath system for 45 min. Then, MIP/MoS_2NPs-MWCNTs/QCM chip was dried with nitrogen gas under vacuum.

Procedure of the analysis

After MIP/MoS_2NP-MWCNT/QCM chip with no analyte molecule was placed in QCM cell, first of all, PBS solution (5.0 mL, pH 6.0) was passed over the chip for 10 min with 1.0 mL min^{-1} flow rate. As a second step, the analyte solution of certain concentration (5.0 mL) was passed onto the chip for 40 min with 1.0 mL min^{-1} flow rate until a constant resonance frequency was obtained. The same process was carried out in analyte solutions of all concentrations within the linearity range. After reaching a certain plateau, during the desorption phase, the "adsorption–desorption–regeneration" cycle was completed by passing 2.0 mol L^{-1} NaCl solution (5.0 mL) for 10 min.

Sample preparation

The rice samples were purchased from a supermarket (Gaziantep/TURKEY). The mixture including rice sample (0.10 g) and acetonitrile (10.0 mL) was prepared in a tube. The centrifugation process was carried out for 15 min at 10,000 rpm, and after the transfer of the diluted upper phase with PBS (5.00 mL) into QCM cell, QCM system was applied for ZEA detection.

Results and discussion

Characterization of MoS_2NPs-MWCNTs and MoS_2NPs

Firstly, XRD results (Fig. S1A) revealed that the obvious XRD peaks attributing to MoS_2NPs were obtained as hexagonal phase in the terms of (002), (101), (103), (105), and (110) crystal planes corresponding to $2\theta = 14.04°$, 33.87°, 40.39°, 49.88°, and 60.11°, respectively [23]. According to MWCNTs' XRD pattern (Fig. S1B), XRD peaks at $2\theta = 7.11°$ and 43.19° relating to (002) and (100) planes, respectively, were attributed to the hexagonal structure of graphite confirming carbon nanotubes' electrochemical conductivity features. In addition, the low XRD peak intensities corresponding to MWCNTs verified the successful decoration of MoS_2NPs into MWCNTs [24]. Moreover, XRD peak having MoS_2NPs-MWCNTs' (002) plane was shifted to positive values in comparison with MoS_2NPs. In conclusion, the lattice expansion in the *c*-axis verified the successful preparation of MoS_2NP-MWCNT nanocomposite. Secondly, Raman spectra (Fig. 1) were recorded for the evaluation of the electronic properties of the produced MoS_2NPs-MWCNTs. The absorption peaks at 409 cm^{-1} (A_{1g}), and 380 cm^{-1} (E^1_{2g}) were in harmony with out-of-plane and in-plane modes of MoS_2NPs, confirming MoS_2NP structure with 2H-MoS_2 [25]. D band at 1350 cm^{-1} and G band at 1592 cm^{-1} were also related to carbon atom with sp^3 hybridization and E^1_{2g} mode, respectively, indicating the presence of MWCNTs [26]. So, the successful synthesis of MoS_2NP-MWCNT nanocomposite was evaluated by Raman measurements.

Then, FTIR spectra of MWCNT and MoS_2NP-MWCNT nanocomposite were recorded (Fig. 2). The absorption peak at about 620 cm^{-1} was resulted from molybdenum disulfide nanoparticles [27]. The absorption bands at 1570 cm^{-1} and 1495 cm^{-1} were also corresponded to

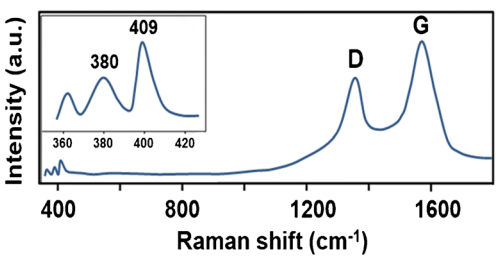

Fig. 1 Raman spectra of MoS_2NPs-MWCNT nanocomposite

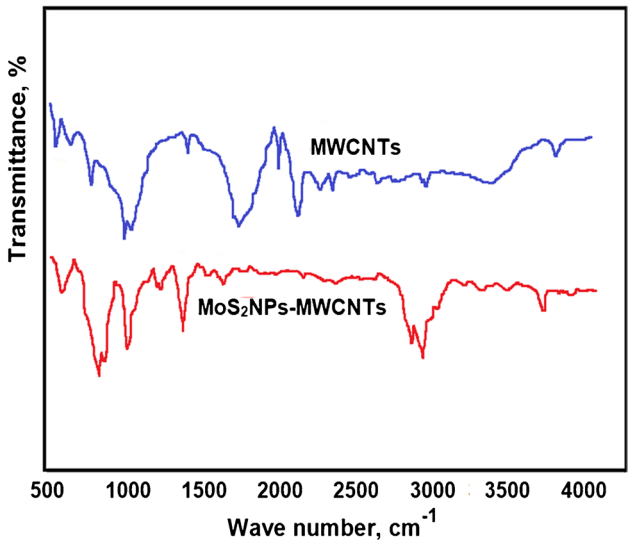

Fig. 2 FTIR spectra of MWCNT and MoS_2NPs-MWCNT nanocomposite

benzenoid ring and –C = C– aromatic ring vibration, providing the presence of MoS_2NPs on MWCNTs [28].

The surface morphological features of MoS_2NP and MoS_2NP-MWCNT nanocomposite were examined by TEM measurements (Fig. 3). The twisted thin layers of MoS_2NPs (Fig. 3A) and MoS_2NPs' uniform grown on nanocomposite and the interconnection interactions between MoS_2NPs and MWCNTs (Fig. 3B) were seen, providing the successful incorporation of MWCNTs between MoS_2NP layers. In addition, these interconnection interactions between MoS_2NPs and MWCNTs caused a three-dimensional structure during hydrothermal process. HRTEM image (Fig. 3C) also demonstrated the space interlayer distances as 0.46 nm and 0.41 nm, respectively. Lastly, SAED pattern (Fig. S2) showed MoS_2NP diffraction rings, confirming a high-crystalline structure in harmony with XRD patterns.

SEM images (Fig. S3) were recorded for MWCNT, MoS_2NP, and MoS_2NP-MWCNT nanocomposite. The tubular structure belonging to MWCNTs seen in Fig. S3A and Fig. S3B revealed MoS_2NPs with wrinkled sheets. The successful incorporation of MWCNTs between MoS_2NP layers was verified with a three-dimensional structure (Fig. S3C). Also, the existence of MoS_2NPs provided an inter-conductive framework, maintaining an efficient interaction between nanocomposite and monomer-analyte complex.

AFM measurements were taken to see the chip surface thickness and surface properties in more detail (Fig. S4). While the surface thickness of bare QCM chip (Fig. S4A) was measured as 3.12 nm, the surface thickness value of the modified QCM chip (Fig. S4B) was determined as 13.79 nm. In addition, the uniform and homogeneous distribution of nanocomposites on the QCM chip shows that a uniform QCM sensor surface can be prepared.

The electrochemical activity properties of MWCNT- and MoS_2NP-MWCNT-modified electrodes were investigated via CV and EIS (Fig. S5). Anodic and cathodic peaks arised at + 0.600 V and + 0.300 V, respectively (curve a of Fig. S5A). After MWCNTs modified GCE (curve b of Fig. S5A), the more electrochemical activity was seen on MWCNTs/GCE because of MWCNTs' large surface area, conductivity, and electronic properties [11, 29]. After the preparation of MoS_2NPs interconnected onto MWCNT surface, the facilitation of charge migration resulted from this synergistic effect caused the more electrochemical activity in comparison with MWCNTs/GCE (curve c of Fig. S5A) [30]. The electrode surface areas of bare GCE, MWCNTs/GCE, and MoS_2NPs-MWCNTs/GCE were indicated by using Randles–Sevcik equation ($n = 6$) [31] and 0.070 ± 0.002 cm^2, 0.114 ± 0.003 cm^2, and 0.234 ± 0.001 cm^2 were found for bare GCE, MWCNTs/GCE, and MoS_2NPs-MWCNTs/GCE, respectively.

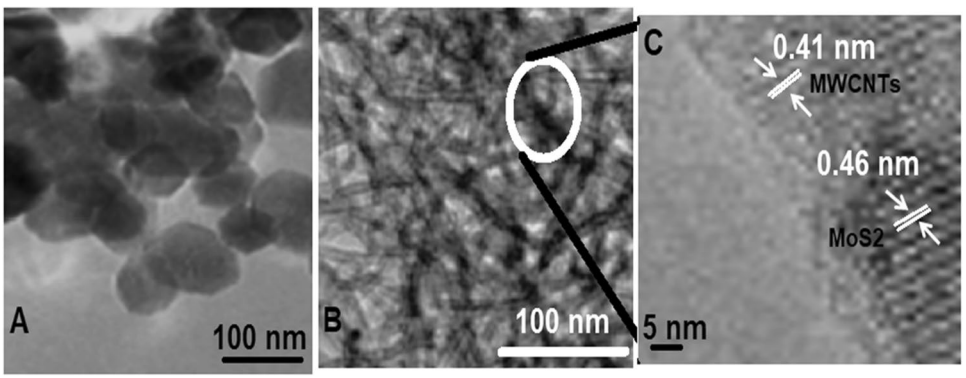

Fig. 3 TEM image of **A** MoS_2NPs, **B** MoS_2NPs-MWCNT nanocomposite, and **C** HRTEM image of MoS_2NP-MWCNT nanocomposite

EIS measurements were applied to confirm the CV results (Fig. S5B). The charge transfer resistance (R_{ct}) values were studied to be 35 Ω for bare GCE (curve a), 25 Ω for MWCNTs/GCE (curve b), and 15 Ω for MoS_2NPs-MWCNTs/GCE (curve c). As a result of least R_{ct} value, the most facile charge transfer occurred on MoS_2NPs-MWCNTs/GCE.

FTIR and AFM characterizations of ZEA-imprinted p(HEMA-MAGA) film on QCM chip

After ZEA desorption from MIP/MoS_2NP-MWCNT/QCM chip, FTIR spectrum of MAGA and HEMA molecules having O–H stretching absorption bands at 3519 cm^{-1}, MAGA molecule having –C–H stretching absorption band at 2983 cm^{-1}, carboxyl-carbonyl stretching absorption band at 1697 cm^{-1}, and –COO– stretching absorption bands at 1455 cm^{-1} and 1439 cm^{-1} are given in Fig. S6A. Thanks to these specific absorption bands, it is possible to say that ZEA-imprinted polymer films on QCM chip surface were successfully formed. Finally, the surface thicknesses of bare QCM chip (Fig. S6B) and ZEA imprinted polymer film on MoS_2NPs-MWCNTs nanocomposite modified QCM chip (Fig. S6C) were detected as 3.12 ± 0.03 and 22.06 ± 0.69 nm, respectively by AFM and UV polymerization on MoS_2NPs-MWCNTs nanocomposite modified QCM chip was carried out successfully.

pH effect on ZEA-imprinted QCM chip

pH effect on ZEA-imprinted QCM chip is investigated in Fig. 4. Since MAGA monomer is based on carboxylic acid, these functional groups can be negatively charged as the pH increases, and the monomer-analyte interaction can be maximum with the increase in pH. However, since the analyte molecule can be converted to the anionic phase at more basic pH values, this interaction decreases at basic pH values. According to Fig. 4, pH 6.0 was preferred for analytical applications since the optimum QCM signal was obtained at pH 6.0.

Linearity range

QCM is one of the most used methods in mass sensitive sensors. The basis of the working principle of these mass sensitive sensors is the "piezoelectric effect" feature of asymmetric crystals such as quartz crystal. If a piezoelectric crystal is connected to a suitable electrical circuit, it vibrates at a fixed frequency depending on the mass and shape of the crystal. QCM shows the changes of mass on gold surface by measuring the frequency in real time [9].

In this study, the linearity range (0.001–0.01 ng mL^{-1}) of MIP/MoS_2NPs-MWCNTs/QCM was firstly formed by using ZEA concentration and QCM signals. Hence, y (nM cm^{-2}) = 1.9209x (C_{ZEA}, ngL^{-1}) − 0.0624 (R^2 = 0.9992) is given in Fig. 5A and 5B. The concentration difference between solution and chip surfaces corresponded to adsorption phenomena. The limit of quantification (LOQ) and LOD values were computed as 1.0 ng L^{-1} (0.001 ng mL^{-1}) and 0.30 ng L^{-1} (0.0003 ng mL^{-1}), respectively (see Supplementary Data for the equations).

Table 1 gives a comparison data considering the sensitivity and linear range values of the recently developed methods for the determination of ZEA. First of all, ZEA determination can be performed more sensitively thanks to the MIP-based QCM sensor in this study in comparison with novel electrochemical methods [31–35]. We can say that the developed QCM sensor is environmentally friendly since the synthesis of MoS_2NPs-MWCNTs takes place in hydrothermal conditions with minimum waste generation and high efficiency during sensor preparation. This not only provides a more livable environment but also allows access to healthier and cleaner foods. Thus, it is possible to say that an important contribution can be carried out in terms of food safety with

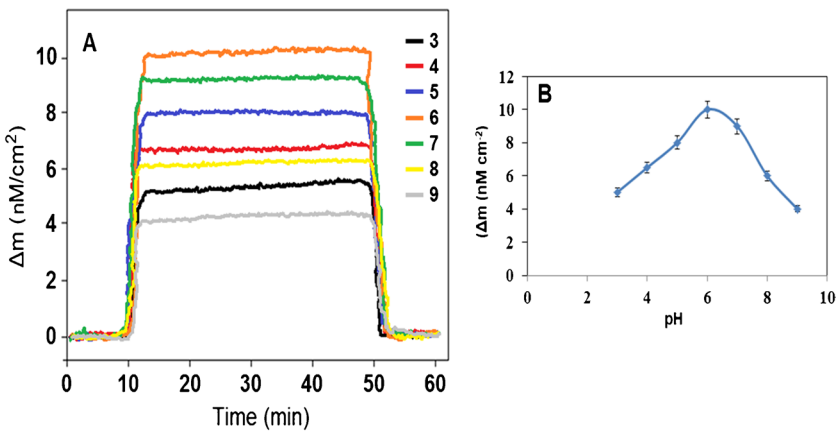

Fig. 4 **A** Sensorgrams for 5.0 ng L^{-1} ZEA in different pHs of PBS and **B** effect of pH on ZEA-imprinted QCM sensor

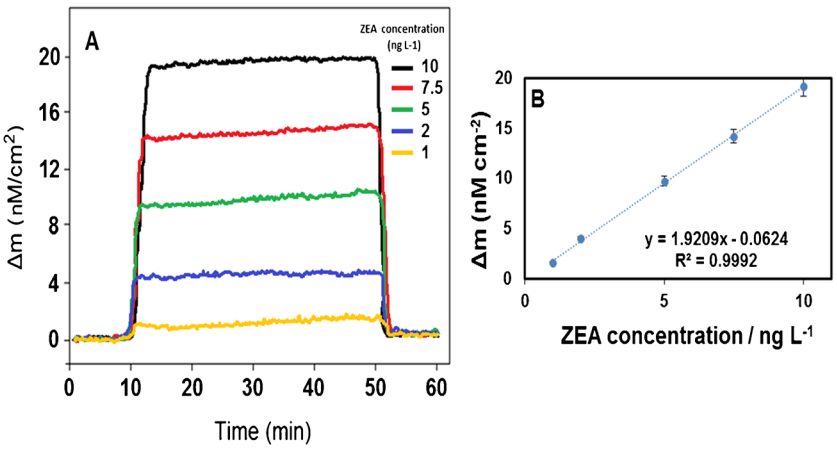

Fig. 5 **A** Effect of ZEA concentration on MIP/MoS_2NP-MWCNT/QCM signals and **B** calibration curve of ZEA concentrations at MIP/MoS_2NPs-MWCNTs/QCM in the presence of pH 6.0 of PBS (from 1.0 to 10.0 ng L^{-1} ZEA): (a) adsorption; (b) desorption; (c) regeneration

Table 1 The comparison of MIP/MoS_2NPs-MWCNTs/QCM's performance with the reported methods for ZEA detection

Material/method	Linear range (ng mL^{-1})	LOD (ng mL^{-1})	Ref
MSN-Rh6G-AuNPs	3.0–200.0	0.0064	[36]
Fluorescence aptasensor	0.01–100.0	0.004	[37]
PCR	6.0–14.0	0.168	[38]
G-quadruplex DNAzyme	1.0–100.0	2.850	[39]
Fluorescence immunoassay	3.51–17.78	0.014	[40]
CS-CNT-Pd	0.25–16.00	0.25	[41]
Gold nanobipyramids	0.02–0.80	0.011	[42]
MIP/MoS_2NPs-MWCNTs/QCM	0.001–0.01	0.0003	This study

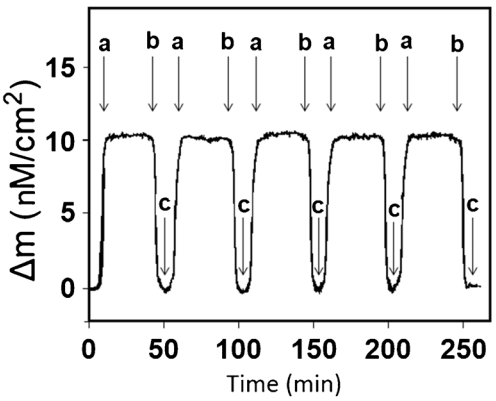

Fig. 6 Repeatability of MIP/MoS_2NPs-MWCNTs/QCM chip: (a) adsorption; (b) desorption; (c) regeneration

this new MIP-based QCM sensor, and it will be more possible in the early diagnosis of diseases that may be caused by mycotoxins. In addition, due to the high selectivity, repeatability, reproducibility, and stability of the developed QCM sensor, ZEA-imprinted QCM sensor is used as a reference method in food chemistry literature for mycotoxin determination.

Recovery assessment

Recovery experiments were performed in real samples such as rice to confirm the validity of MIP/MoS_2NPs-MWCNTs/QCM. First of all, the analysis was carried out thanks to the ZEA-imprinted QCM sensor without adding standard ZEA solution to the rice samples and the value of 1.27 ± 0.09 ng L^{-1} was found (Table S1). Then, ZEA analyses were performed after adding ZEA solutions at increasing concentrations (2.00, 4.00, and 6.00 ng L^{-1}) to rice samples and as a result, values close to 100% prove a high recovery (Table S1, see Supplementary Data).

Selectivity, repeatability, reusability, and stability of MIP/MoS_2NPs-MWCNTs/QCM

For selectivity experiments of MIP/MoS_2NPs-MWCNTs/QCM, 3 common mycotoxins (AFB1, FB1, OTA) were detected. QCM signals (nM cm^{-2}) were obtained for 5.0 ng L^{-1} ZEA, 500.0 ng L^{-1} AFB1, 500.0 ng L^{-1} FB1, and 500.0 ng L^{-1} OTA on MIP/MoS_2NPs-MWCNTs/QCM and NIP/MoS_2NPs-MWCNTs/QCM (Fig. S7A and S7B). These QCM signals are given in Table S2 including selectivity coefficient (k) and relative selectivity coefficient (k') values. It was concluded that MIP/MoS_2NPs-MWCNTs/QCM was 10.00, 20.00, and 40.00 times more selective for ZEA than AFB1, FB1, and OTA, respectively, because of specific nano-cavities of ZEA on QCM electrode surface. Thus, a

reliable and selective ZEA-imprinted QCM sensor has been developed for ZEA analysis.

Five cycles were repeated in existence of 5.0 ng L^{-1} ZEA for short-term repeatability of MIP/MoS_2NPs-MWCNTs/QCM chip and the repeatable QCM signals with 0.59% of relative standard deviation (RSD) were obtained during the cycles (Fig. 6).

Reusability test of ZEA-imprinted QCM sensor was also evaluated thanks to measurements obtained as a result of using the same ZEA-imprinted sensor at 30 times after cleaning. RSD value of the obtained results was 0.93%, confirming a high degree of reusability.

Long-term stability test of only one MIP/MoS_2NPs-MWCNTs/QCM was evaluated for 7 weeks. The observed QCM signals on seventh week was ~ 98.83% of the QCM signals on first week. Thus, this situation provided long-term stability of ZEA-imprinted QCM sensor.

Conclusions

In this study, the presented method, QCM chip based on molecular imprinted polymer, was successfully performed for the determination of ZEA in rice samples. The prepared MoS_2NP-MWCNT nanocomposite revealed the excellent QCM chip material owing to the synergistic effect between MoS_2NPs and MWCNTs. In addition, the developed ZEA-imprinted QCM sensor based on MoS_2NP-MWCNT nanocomposite demonstrated good selectivity, repeatability, reusability, and stability. This sensor can detect ZEN in linearity range of 1.0–10.0 ng L^{-1} with LOD of 0.30 ng L^{-1}. The MIP-based QCM sensor also has other advantages such as repeatability and stable preparation method. Moreover, this prepared sensor can be used as an alternative method to detect different mycotoxins and reveal their harmful effects.

Supplementary Information The online version contains supplementary material available at https://doi.org/10.1007/s00604-023-05842-8.

Data availability The data that support the findings of this study are available on request from the corresponding author.

Declarations

Conflict of interest The authors declare no competing interests.

References

1. Wu Z, Pu H, Sun D-W (2021) Fingerprinting and tagging detection of mycotoxins in agri-food products by surface-enhanced Raman spectroscopy: principles and recent applications. Trends Food Sci Technol 110:393–404
2. Hassan MM, Zareef M, Xu Y, Li H, Chen Q (2021) SERS based sensor for mycotoxins detection: challenges and improvements. Food Chem 344:128652
3. Labuda R, Parich A, Berthiller F, Tančinová D (2005) Incidence of trichothecenes and zearalenone in poultry feed mixtures from Slovakia. Int J Food Microbiol 105(1):19–25
4. Marroquín-Cardona AG, Johnson NM, Phillips TD, Hayes AW (2014) Mycotoxins in a changing global environment – a review. Food Chem Toxicol 69:220–230
5. Rodríguez-Carrasco Y, Moltó JC, Mañes J, Berrada H (2014) Development of a GC–MS/MS strategy to determine 15 mycotoxins and metabolites in human urine. Talanta 128:125–131
6. Keskin E, Eyupoglu OE (2023) Determination of mycotoxins by HPLC, LC-MS/MS and health risk assessment of the mycotoxins in bee products of Turkey. Food Chem 400:134086
7. Abreu DCP, Vargas EA, da Silva Oliveira FA, Madureira FD, Gomes MB, Bazzana MJF, Saczk AA (2023) Validation and estimation of uncertainty of an LC-MS/MS method for the simultaneous determination of 34 mycotoxins in cocoa beans. Food Chem 399:133902
8. Pohanka M (2018) Overview of piezoelectric biosensors, immunosensors and DNA sensors and their applications. Materials 11(3):448
9. Kadirsoy S, Atar N, Yola ML (2020) Molecularly imprinted QCM sensor based on delaminated MXene for chlorpyrifos detection and QCM sensor validation. New J Chem 44(16):6524–6532
10. Verma D, Chauhan D, Das Mukherjee M, Ranjan KR, Yadav AK, Solanki PR (2021) Development of MWCNT decorated with green synthesized AgNps-based electrochemical sensor for highly sensitive detection of BPA. J Appl Electrochem 51(3):447–462
11. Agüí L, Yáñez-Sedeño P, Pingarrón JM (2008) Role of carbon nanotubes in electroanalytical chemistry: a review. Anal Chim Acta 622(1):11–47
12. Lahiff E, Lynam C, Gilmartin N, O'Kennedy R, Diamond D (2010) The increasing importance of carbon nanotubes and nanostructured conducting polymers in biosensors. Anal Bioanal Chem 398(4):1575–1589
13. Merkoçi A, Pumera M, Llopis X, Pérez B, del Valle M, Alegret S (2005) New materials for electrochemical sensing VI: carbon nanotubes. TrAC Trends Anal Chem 24(9):826–838
14. Huang K-J, Wang L, Li J, Liu Y-M (2013) Electrochemical sensing based on layered MoS2–graphene composites. Sensor Actuat B-Chem 178:671–677
15. Li J, Yang Z, Tang Y, Zhang Y, Hu X (2013) Carbon nanotubes-nanoflake-like SnS2 nanocomposite for direct electrochemistry of glucose oxidase and glucose sensing. Biosens Bioelectron 41:698–703
16. Li Y, Xu C-Y, Hu P, Zhen L (2013) Carrier control of MoS2 nanoflakes by functional self-assembled monolayers. ACS Nano 7(9):7795–7804
17. Yin Z, Li H, Li H, Jiang L, Shi Y, Sun Y, Lu G, Zhang Q, Chen X, Zhang H (2012) Single-layer MoS2 phototransistors. ACS Nano 6(1):74–80
18. Ma G, Peng H, Mu J, Huang H, Zhou X, Lei Z (2013) In situ intercalative polymerization of pyrrole in graphene analogue of MoS2 as advanced electrode material in supercapacitor. J Power Sources 229:72–78
19. Yola ML, Atar N (2017) A review: molecularly imprinted electrochemical sensors for determination of biomolecules/drug. Curr Anal Chem 13(1):13–17
20. Yola ML (2022) Carbendazim imprinted electrochemical sensor based on CdMoO4/g-C3N4 nanocomposite: application to fruit juice samples. Chemosphere 301:134766
21. Karaman C, Karaman O, Atar N, Yola ML (2022) A molecularly imprinted electrochemical biosensor based on hierarchical $Ti_2Nb_{10}O_{29}$ (TNO) for glucose detection. Microchim Acta 189:24

22. Yadav AK, Verma D, Solanki PR (2021) Electrophoretically deposited L-cysteine functionalized MoS2@MWCNT nanocomposite platform: a smart approach toward highly sensitive and label-free detection of gentamicin. Mater Today Chem 22:100567
23. Liu Y-R, Hu W-H, Li X, Dong B, Shang X, Han G-Q, Chai Y-M, Liu Y-Q, Liu C-G (2016) One-pot synthesis of hierarchical Ni2P/MoS2 hybrid electrocatalysts with enhanced activity for hydrogen evolution reaction. Appl Surf Sci 383:276–282
24. Huang K-J, Liu Y-J, Wang H-B, Wang Y-Y, Liu Y-M (2014) Sub-femtomolar DNA detection based on layered molybdenum disulfide/multi-walled carbon nanotube composites, Au nanoparticle and enzyme multiple signal amplification. Biosens Bioelectron 55:195–202
25. Lee C, Yan H, Brus LE, Heinz TF, Hone J, Ryu S (2010) Anomalous lattice vibrations of single- and few-layer MoS2. ACS Nano 4(5):2695–2700
26. Yola ML, Atar N (2019) Simultaneous determination of beta-agonists on hexagonal boron nitride nanosheets/multi-walled carbon nanotubes nanocomposite modified glassy carbon electrode. Mater Sci Eng C-Mater Biol Appl 96:669–676
27. Silambarasan K, Archana J, Harish S, Navaneethan M, Ganesh RS, Ponnusamy S, Muthamizhchelvan C, Hara K (2020) One-step fabrication of ultrathin layered 1T@2H phase MoS2 with high catalytic activity based counter electrode for photovoltaic devices. J Mater Sci Technol 51:94–101
28. Yilmaz E, Baghban N, Soylak M (2023) Solid-phase extraction (SPE) of salmon sperm DNA using a polyaniline@molybdenum(IV) sulfide@multiwalled carbon nanotubes (MWCNTs) nanocomposite with spectrophotometric detection. Anal Lett 56(10):1632–1645
29. Xu Q, Wang S-F (2005) Electrocatalytic oxidation and direct determination of L-tyrosine by square wave voltammetry at multiwall carbon nanotubes modified glassy carbon electrodes. Microchim Acta 151(1):47–52
30. Bölükbaşı ÖS, Yola BB, Boyacıoğlu H, Yola ML (2022) A novel paraoxon imprinted electrochemical sensor based on MoS2NPs@MWCNTs and its application to tap water samples. Food Chem Toxicol 163:112994
31. Ansari S, Ansari MS, Satsangee SP, Alam MG, Jain R (2023) Electrochemical sensing platform based on ZrO2/BiVO4 nanocomposite for gastro-prokinetic drug in human blood serum. J Nanostructure Chem 13(3):361–375
32. Ansari S, Ansari MS, Satsangee SP, Jain R (2021) Bi2O3/ZnO nanocomposite: synthesis, characterizations and its application in electrochemical detection of balofloxacin as an anti-biotic drug. J Pharm Anal 11(1):57–67
33. Ansari S, Ansari MS, Satsangee SP, Jain R (2019) WO3 decorated graphene nanocomposite based electrochemical sensor: a prospect for the detection of anti-anginal drug. Anal Chim Acta 1046:99–109
34. Ansari S, Ansari MS, Devnani H, Satsangee SP, Jain R (2018) CeO2/g-C3N4 nanocomposite: a perspective for electrochemical sensing of anti-depressant drug. Sensor Actuat B-Chem 273:1226–1236
35. Devnani H, Ansari S, Satsangee SP, Jain R (2017) ZrO2-graphene-chitosan nanocomposite modified carbon paste sensor for sensitive and selective determination of dopamine. Mater Today Chem 4:17–25
36. Guo Z, Gao L, Yin L, Arslan M, El-Seedi HR, Zou X (2023) Novel mesoporous silica surface loaded gold nanocomposites SERS aptasensor for sensitive detection of zearalenone. Food Chem 403:134384
37. Ma P, Guo H, Ye H, Zhang Y, Wang Z (2023) Aptamer-locker probe coupling with truncated aptamer for high-efficiency fluorescence polarization detection of zearalenone. Sensor Actuat B-Chem 380:133356
38. Ma L, Zhang X, Peng Y, Chen W, Xiao Y, Fang H, Yang H, Zhou Y (2023) Based on intervening PCR for detection of alkaline phosphatase and zearalenone. Microchem J 186:108314
39. Guan Y, Ma J, Neng J, Yang B, Wang Y, Xing F (2023) A novel and label-free chemiluminescence detection of zearalenone based on a truncated aptamer conjugated with a G-quadruplex DNAzyme. Biosensors 13(1):118
40. Wu S, Zhang X, Chen W, Zhang G, Zhang Q, Yang H, Zhou Y (2023) Alkaline phosphatase triggered ratiometric fluorescence immunoassay for detection of zearalenone. Food Control 146:109541
41. Kumar VS, Kummari S, Catanante G, Gobi KV, Marty JL, Goud KY (2023) A label-free impedimetric immunosensor for zearalenone based on CS-CNT-Pd nanocomposite modified screen-printed disposable electrodes. Sensor Actuat B-Chem 377:133077
42. Zhang Q, Zhang X, Zhang G, Chen W, Wu S, Yang H, Zhou Y (2023) Multicolor immunosensor for detection of zearalenone based on etching Au NBPs mediated by HRP. J Food Compost Anal 115:105014